

Small Molecule Elimination from Group IVB (Ti, Zr, Hf) Amido Complexes

Thomas R. Cundari^{*1} and Mark S. Gordon²

Contribution from the Departments of Chemistry, Memphis State University, Memphis, Tennessee 38152, and Iowa State University, Ames, Iowa 50011

Received November 16, 1992

Abstract: An ab initio quantum chemical analysis of HX (X = H, CH₃, Cl, NH₂, SiH₃) elimination by group IVB (Ti, Zr, Hf) amidos (H₂(X)M—NH₂ → H₂M=NH + HX), of interest in the context of CVD precursor design, is reported. Several deductions may be drawn from the calculations. First, in the transition state (TS) for HX elimination, electropositive and electroneutral X give rise to metal–transannular hydrogen (H_t) distances only slightly longer than normal metal–terminal hydride bonds lengths, while electronegative X groups yield substantially longer MH_t distances. Second, the HX elimination barrier ($\Delta H^\ddagger_{\text{elim}}$) is lower when HX is polarized H^{δ-}–X^{δ+} (X = SiH₃) or nonpolar (X = H). Third, a plot of calculated $\Delta H^\ddagger_{\text{elim}}$ versus MH_t distances in the TS for a given metal shows good correlation between low HX elimination barriers and short MH_t distance in the TS. Fourth, analysis of the electronic structure along the intrinsic reaction coordinate (IRC) supports the importance of N—H...M agostic interactions preceding N—H scission. Fifth, the IRC shows the MH_t distance decreasing as H_t is transferred from N to X, reaching a minimum when the transfer is roughly half complete, and then increasing once more as HX is eliminated. These results point to the leaving group (X) playing a crucial role in tuning the bonding and energetics of the TS, and thus the rate of HX elimination. The results lead to the conclusion that materials precursors designed to enhance MH_t interaction, through the intermediacy of X, in the TS and along the reaction coordinate will lead to lower activation barriers to XH elimination.

Introduction

The elimination of small molecules (XH) from saturated organometallic complexes (L_nM(X)—E(H)) to produce coordinatively unsaturated, multiply bonded species (L_nM=E) is a reaction of fundamental importance in the synthesis of solid-state, advanced materials by chemical vapor deposition (CVD) techniques.³ The deposition of main-group (MG), transition metal (TM), and mixed transition metal–main group (TM-MG) materials is an area of considerable interest.^{4,5} Computational chemistry has played an important role in understanding the structure of intermediates and transition states, as well as the dynamics of reaction pathways, pertinent to main-group CVD;⁶ however, computational studies of mechanisms germane to the synthesis of TM-MG materials are virtually nonexistent.⁷ The rational design of improved TM-MG precursors (e.g., those which can be processed at lower temperatures) for CVD will result from a better understanding of the chemical factors affecting the crucial elimination process.

TM-nitrides are a prominent family of TM-MG materials.⁸ Traditionally, TM-nitrides have been synthesized by direct

reaction of metal and NH₃ at elevated temperatures.⁹ TM-nitrides have been investigated for a variety of catalysis applications, including the hydrodenitrogenation of petroleum feedstocks.¹⁰ Transition metal nitrides make attractive materials because of their hardness and thermal resistance, coupled with metal-like electrical conductivity and heat capacity.⁸ Preparation from the corresponding oxide and ammonia has recently been reported as a convenient method for the synthesis of high surface area TM-nitrides.¹⁰ Reaction of primary amines (RNH₂) with TiCl₄ has long been known to result in complex mixtures, which include nitride materials; imido (L_nM=NR) and amido (L_{n+1}M—NHR) complexes have been envisaged as intermediates in these reactions.¹¹ Hoffman et al. have synthesized solid-state TM-nitrides by the addition of volatile amines (e.g., ammonia) to dimethyl-amido complexes; imido complexes are also thought to be formed in these reactions.¹² Winter et al. recently provide perhaps the best evidence (through a combination of X-ray crystallographic and mass spectral data) for the intermediacy of imido complexes in the reaction of TiCl₄ and *tert*-butylamine to yield solid-state TiN.¹³

Given a continuing interest in high-valent TM-MG complexes,^{7,14} a computational study of the elimination of small molecules (XH) from group IVB (M = Ti, Zr, Hf) amidos (L_nM(NH₂)(X)) was initiated. Si analogues are also included to gauge differences between MG and TM-MG compounds. Previous work on CH₄ and H₂ elimination^{7,14b} suggest that the effect of the ancillary ligands (L_n) is primarily steric. Thus, the purpose of the present contribution is to assess the consequences of leaving

(1) E-mail: cundarit@memstvx1.memst.edu.

(2) E-mail: mark@si.fi.ameslab.gov.

(3) *Mechanisms of Reactions of Organometallic Compounds with Surfaces*; Cole-Hamilton, D. J., Williams, J. O., Eds.; NATO ASI Series B; Plenum: New York, 1988; Vol. 198.

(4) Perhaps the most thoroughly studied main-group systems involve the deposition of Si-based, III–V (e.g., GaAs) and II–VI (e.g., ZnS) materials. (a) Si: Jasinsky, J. M.; Gates, S. M. *Acc. Chem. Res.* **1991**, *24*, 9. (b) III–V: Cowley, A. H.; Benac, B. L.; Ekerdt, J. G.; Jones, R. A.; Kidd, K. B.; Lee, J. Y.; Miller, J. E. *J. Am. Chem. Soc.* **1988**, *110*, 6248 and references therein. (c) II–VI: Jones, A. C.; Wright, P. J.; Cockayne, B. J. *Cryst. Growth* **1991**, *107*, 207. Brennan, J. G.; Siegrist, T.; Carroll, P. J.; Straczynski, S. M.; Reynder, P.; Brus, L. E.; Steigerwald, M. L. *Chem. Mater.* **1990**, *2*, 403.

(5) Typical deposition applications for TM–MG include: (a) TiC: Girolami, G. S.; Jensen, J. A.; Pollina, D. M.; Williams, W. S.; Kaloyeros, A. C.; Alloca, C. M. *J. Am. Chem. Soc.* **1987**, *109*, 1579. (b) WC: Chisholm, M. H.; Caulton, K. G.; Xue, X. *Chem. Mater.* **1991**, *3*, 384. (c) TiC: Derre, A.; Ducarroir, M.; Teysandir, F. *J. Electrochem. Soc.* **1989**, *136*, 835. (d) TM oxides: Bradley, D. C. *Chem. Rev.* **1989**, *89*, 1317.

(6) For applications to Si-based materials see: Gordon, M. S.; Francisco, J.; Schlegel, H. B. *Adv. Silicon Chem.*, in press.

(7) H₂ elimination from Zr-amido compounds: Cundari, T. R. *Int. J. Quantum Chem., Proc. 1992 Sanibel Symp.* **1992**, *26*, 793.

(8) Oyama, S. T. In *Catalysis*, Royal Society of Chemistry: Oxford, 1982; Vol. 5.

(9) Cotton, F. A.; Wilkinson, G. *Advanced Inorganic Chemistry*, 5th ed.; Wiley: New York, 1988; p 269.

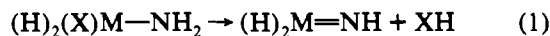
(10) (a) Oyama, S. T.; Schlatter, J. C.; Metcalfe, J. E.; Lambert, J. *I & EC Res.* **1988**, *27*, 1639, 1649. (b) Boudart, M.; Oyama, S. T. *Proc. 12th Iberoamerican Symp. Cat.*, submitted for publication.

(11) (a) Maya, L. *Inorg. Chem.* **1986**, *25*, 4213. (b) Saeki, Y.; Matsuzaki, R.; Yajima, A.; Akiyama, M.; Yokohama, N.; Hinode, K.; Homma, Y. *J. Electrochem. Soc.* **1989**, *136*, 882.

(12) Fix, R. M.; Gordon, R. G.; Hoffman, D. M. *J. Am. Chem. Soc.* **1990**, *112*, 7833.

(13) Winter, C. H.; Sheridan, P. H.; Lewkebandara, T. S.; Heeg, M. J.; Proscia, J. W. *J. Am. Chem. Soc.* **1992**, *114*, 1095.

group (X) and metal (M) modification on HX elimination from transition metal amido complexes, by studying the reactions:



We wish to understand the factors which control the barrier to elimination of HX in eq 1. Lower kinetic barriers to elimination can lead to lower CVD processing temperatures (resulting in lower energy costs, better control of surface morphology, and the need for less expensive equipment) or faster rates at a given temperature (and thus faster processing times).

Computational Methods

Calculations employed the ab initio program GAMES^{15a} in sequential, vector (National Center for Supercomputing Applications), and parallel^{15b} (Oak Ridge National Laboratories) modes, the latter using up to 128 nodes on the iPSC/860 parallel supercomputer. Effective core potentials (ECPs) replace chemically unimportant core orbitals and make calculations feasible for all rows of the transition series. ECPs and valence basis sets¹⁶ are used for heavy atoms while H's are described with the -31G basis set. Basis sets for heavy, MG elements are augmented with a set of d polarization functions.¹⁷ The combination of ECPs, basis sets, and level of theory employed here has been successfully tested for a large number of TM species.^{7,14} Geometry optimizations are done at the restricted Hartree-Fock (RHF) level for closed-shell singlets. Vibrational frequencies are calculated at stationary points to identify them as minima (all positive frequencies) or transition states (one imaginary frequency). The intrinsic reaction coordinate (IRC),¹⁸ the steepest descent path from the transition state (TS), is used to assess which TS connects which reactant and products. The steepest descent algorithm (step size = 0.15 bohr-amu^{1/2}) used to follow the IRC is that of Ishida et al.,¹⁹ with the stabilization method described by Schmidt et al.^{19b,c}

Previous work^{7,14} clearly demonstrated that d⁰ complexes similar to those studied here are well described at the single-determinant level; multiple bonds involving third-row main-group elements (e.g., Si) require more sophisticated treatments.^{14f,g} More extensive studies of H₂⁷ and CH₄^{14b} elimination confirm the appropriateness of a single-determinant description at the transition states and along the intrinsic reaction coordinate. Thus, geometric parameters are expected to be accurately predicted since a flexible basis set is used. Calculated energetic will usually be poor if electron correlation is ignored. For species described well at the single-determinant level of theory, the correlation contribution can be treated as a perturbation to the single-determinant energy. For this reason, the correlation energy is calculated using second-order perturbation theory within the Moller-Plesset (MP2) formulation.²⁰ Core electrons are not included in the MP2 active space. All quoted energies are determined at the MP2 level of theory using the RHF optimized geometries with zero-point-energy (ZPE) corrections included. Relative energies are calculated versus separated products and reactants. This approach has been found to give good agreement with experimental

(14) TM-nitrogen,^{14a,b} TM-carbon,^{14c-c} and TM-silicon^{14f,g} TM-phosphorus^{14h} complexes: (a) Cundari, T. R. *J. Am. Chem. Soc.* **1992**, *114*, 7879. (b) Cundari, T. R. *J. Am. Chem. Soc.* **1992**, *114*, 10 557. (c) Cundari, T. R.; Gordon, M. S. *J. Am. Chem. Soc.* **1991**, *113*, 5231. (d) Cundari, T. R.; Gordon, M. S. *Organometallics* **1992**, *11*, 55. (e) Cundari, T. R.; Gordon, M. S. *J. Am. Chem. Soc.* **1992**, *114*, 539. (f) Cundari, T. R.; Gordon, M. S. *J. Phys. Chem.* **1992**, *96*, 631. (g) Cundari, T. R.; Gordon, M. S. *Organometallics* **1992**, *11*, 3122. (h) Tanaka, K.; Gordon, M. S. In preparation.

(15) (a) GAMES: Schmidt, M. W.; Baldrige, K. K.; Boatz, J. A.; Jensen, J. H.; Koseki, S.; Gordon, M. S.; Nguyen, K. A.; Windus, T. L.; Elbert, S. T. *QCPE Bull.* **1990**, *10*, 52. (b) Further discussion of the implementation of GAMES to run on parallel architectures are to be published in: Schmidt, M. W.; Baldrige, K. K.; Boatz, J. A.; Jense, J. H.; Koseki, S.; Matsunaga, N.; Gordon, M. S.; Nguyen, K. A.; Su, S.; Windus, T. L.; Elbert, S. T.; Montgomery, J.; Dupuis, M. *J. Comput. Chem.*, to be submitted.

(16) Krauss, M.; Stevens, W. J.; Basch, H.; Jasien, P. G. *Can. J. Chem.* **1992**, *70*, 612.

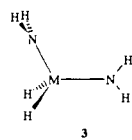
(17) Pople, J. A.; Hehre, W. J.; Radom, L.; Schleyer, P. v. R. *Ab Initio Molecular Orbital Theory*; Wiley: New York, 1986.

(18) Truhlar, D. G.; Gordon, M. S. *Science* **1990**, *249*, 491.

(19) (a) Ishida, K.; Morokuma, K.; Komornicki, A. *J. Chem. Phys.* **1977**, *66*, 2153. (b) Schmidt, M. W.; Gordon, M. W.; Dupuis, M. *J. Am. Chem. Soc.* **1985**, *107*, 2585. (c) Garrett, B. C.; Redmon, M. J.; Steckler, R.; Truhlar, D. G.; Baldrige, K. K.; Bartol, D.; Schmidt, M. W.; Gordon, M. S. *J. Phys. Chem.* **1989**, *93*, 2888.

(20) Moller, C.; Plesset, M. S. *Phys. Rev.* **1934**, *46*, 618.

Table I. Geometries of Amido Reactants^a



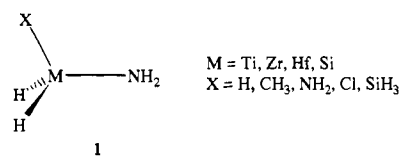
		R_{MX} (Å)	R_{MN} (Å)	θ_{XMN} (deg)	β (deg)
X = H	Ti	1.71	1.88	112	0
	Zr	1.88	2.03	108	0
	Hf	1.87	2.00	108	0
	Si	1.49	1.73	108	-34
X = CH ₃	Ti	2.07	1.89	111	0
	Zr	2.24	2.04	108	0
	Hf	2.23	2.01	108	0
	Si	1.89	1.73	116	-31
X = NH ₂	Ti	1.89	1.89	105	+1
	Zr ^b	2.04	2.05	110	-1
	Hf	2.02	2.02	110	-1
	Si	1.73	1.73	120	-30
X = Cl	Ti	2.24	1.86	117	0
	Zr	2.41	2.01	114	0
	Hf	2.39	2.00	115	0
	Si	2.09	1.71	114	-31
X = SiH ₃	Ti	2.61	1.88	107	-1
	Zr	2.82	2.03	107	-1
	Hf	2.82	2.00	108	-2
	Si	2.38	1.74	115	-34

^a Other calculated bond lengths: $R_{NH} = 1.01 \pm 0.01$ Å; $R_{CH} = 1.01 \pm 0.01$ Å; $R_{SiH} = 1.49 \pm 0.01$ Å. Bond angles are as expected from VSEPR, except as noted in text. ^b The MN bonds are unequal in Zr(NH₂)₂(H)₂, since the NH₂ groups are inequivalent, **3**. The other bis(amido) possess this geometry, but MN bond lengths are the same to within 0.01 Å. The β is for the NH₂ bisected by the C_v plane; the other has $\beta = 0^\circ$ by symmetry; see text for definition of B.

methane elimination barriers for TM species^{14b} and has been used with great success for MG analogues of the reactions to be studied here.⁶

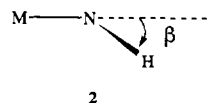
Results

1. Reactants and Products. The reactants are pseudotetrahedral amidos of the general form (H)₂M(X)(NH₂), with the metals (M) and leaving groups (X) shown in **1**. Leaving groups



were chosen to obtain a representative selection of electronegative, electropositive, and electroneutral groups. The ancillary ligands were modeled with H to make the study of larger leaving groups computationally feasible. The structures of the amidos are quite standard. Metal-liquid bond lengths are essentially identical with those reported elsewhere,¹⁴ while angles are near those expected from simple VSEPR considerations (Table I).

The main difference between TM and Si amidos is in the bonding of the amido ligand. The bonding about the TM amido N is trigonal planar or very nearly so. The calculated minima for Si-amido compounds show a less planar, more pyramidal coordination geometry about the amido N. The amount of bending is measured by the flap angle (β , **2**), the acute angle



between the M-N bond vector and the NH₂ plane. For TM-amidos, $\beta \approx \pm 2^\circ$ while $\beta \approx -32^\circ$ for Si-amidos. A negative β indicates that the amido pyramidalizes so that the N lone pair points away from the X group and is gauche to the M-H bonds.

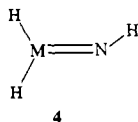
Table II. Geometries of Imido Products, $(\text{H})_2\text{M}=\text{NH}^a$

	R_{MN} (Å)	R_{MH} (Å)	Θ_{HMH} (deg)	Θ_{MNH} (deg)
Ti	1.65	1.77	127	180
Zr	1.80	1.93	121	175
Hf	1.79	1.93	121	175
Si	1.58	1.49	112	122

^a Pertinent geometric details calculated at the RHF level using the methods described in Computational Methods.

For ideal trigonal-planar and tetrahedral coordination, $\beta = 0^\circ$ and $\approx 57.5^\circ$, respectively, putting the Si systems midway between these extremes. Note that theory²¹ indicates a small inversion barrier at N (≈ 1 kcal mol⁻¹) in H_3SiNH_2 , while experimentally characterized di- and trisilyl amines are planar about the central N.²²

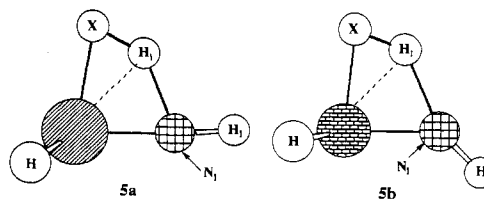
The products of reaction 1 are a small molecule (X-H) and the parent imido complex, $(\text{H})_2\text{M}=\text{NH}$, **4**. As for the reactants,



the geometries of imido compounds (Table II) have been discussed in the literature, Table II.^{14b,23} The only major difference in the imido products is between the TM-imidos and their Si analogues; the M-N-H angle is near linear ($\geq 175^\circ$) for the TM-imidos, and significantly bent for $\text{H}_2\text{Si}=\text{NH}$. The Si=N-H angle in the Si-imido (122°) is suggestive of an sp^2 N, a formal silicon-nitrogen double bond, and a N lone pair on the N. Localization of the canonical RHF molecular orbitals²⁴ supports this view of the bonding in $\text{H}_2\text{Si}=\text{NH}$. The linear coordination mode in the TM cases has been interpreted as signifying a triple bond formulation for the metal-imido linkage.²⁵ An extensive computational analysis of TM-imido complexes has been reported and indicates that the description of the metal-nitrogen linkage is significantly more complex than a single resonance structure description.^{14a}

2. Transition States. Extensive mechanistic studies on high-valent TM complexes supports a four-center TS for HX activation, arising from [2 + 2] addition of X-H across the appropriate transition metal-ligand bond.²⁶ Thus, the microscopic reverse reaction, HX elimination, will pass through the same four-center TS. In this respect, early, high-valent TMs differ from late, low-valent TM complexes, in which the experimental and computational evidence favor 1,1-addition/elimination pathways involving oxidative addition.²⁷

The optimized four-center TSs are "kite-shaped" with one obtuse angle about the H being transferred in the TS (H_i) and three acute angles. The calculated four-center TS geometries are collected in Table III and have the general shapes shown in **5a** (for TM systems) and **5b** (for Si systems). Exocyclic bond lengths and angles differ little from values in the products and reactants. Extensive work^{6,23} on the elimination of small molecules from Si compounds has indicated that 1,1-elimination pathways are preferred, so that the Si TSs shown in Table III may not be the lowest connecting reactants and products. As for the reactants and products, there is a degree of structural similarity between the various transition metals, the most noticeable difference being in the bonding about the imido N (N_i , the cross-hatched circles

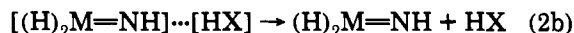
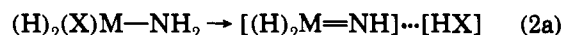


in **5**), nearly linear in the TMs (**5a**) and more significantly bent for the Si cases (**5b**).

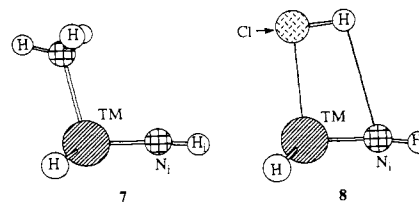
For TM species, M-N-H_i angles (H_i is the hydrogen attached to N_i , **5**) and M-N_i bond lengths in the transition states, Table III, are close to those of the imido product, Table II, suggesting a late TS for HX elimination; the situation is less clear in this regard to Si analogues. A late TS is consistent with the endothermicity (Table IV) of the elimination reaction. For a given X, it is generally found that (a) the overall reaction (1) is endothermic and (b) the endothermicity increases in the order $\text{Ti} < \text{Zr} < \text{Hf} < \text{Si}$, with the last inequality reversed for $\text{X} = \text{NH}_2$ and Cl. For a given metal, the endothermicity of the reaction increases in the order $\text{H} \approx \text{SiH}_3 < \text{CH}_3 \ll \text{NH}_2 < \text{Cl}$. There is a certain degree of variation in comparable bond lengths and angles in the TSs in Table III for a given metal as a function of X. For example, the elimination of NH_3 and HCl would seem to occur earlier along a hypothetical reaction coordinate than the others, as evidenced by their smaller M-N-H_i and larger M-N-H_i angles (H_i is the transannular hydrogen in the TS, **5**), Table III, but this is in contrast to their very large endothermicities shown in Table IV. Recent experiments by Wolczanski et al. on α -elimination of hydrocarbons from tris(amido)alkyl Zr complexes suggest that the TS is more variable in its position along the reaction coordinate (i.e., later versus earlier) than previously envisioned for α -elimination in high-valent transition metal systems.²⁸ These experiments challenge the standard view of the rigidly "late" TS for α -elimination (and hence an "early" TS for the microscopic reverse, [2 + 2] addition). The present results, albeit for widely varying X groups, are in concurrence with this conclusion.

Although similar in geometry, the energetic content of the transition states varies considerably as a function of M and X. Calculated enthalpic data are given in Table IV. With the exception of $\text{X} = \text{SiH}_3$, the calculated activation enthalpies are in the order one would predict from the Hammond postulate, based on the endothermicity trends discussed above.

When HX is a good Lewis acid ($\text{X} = \text{Cl}$) or base ($\text{X} = \text{NH}_2$), a strongly bound adduct is expected prior to separation of products. In such cases HX elimination can be envisaged in two steps: HX bond formation, eq 2a, followed by dissociation of HX, eq 2b. In



the case of NH_3 elimination, the ammonia coordinates to the metal of the imido, **7**, with an appreciable binding energy, ≈ 40



(28) (a) Wolczanski, P. T. (Department of Chemistry, Cornell). Personal communication. (b) Cummins, C. C.; Baxter, S. M.; Wolczanski, P. T. *J. Am. Chem. Soc.* **1988**, *110*, 8729.

(21) Gordon, M. S. *Chem. Phys. Lett.* **1986**, *126*, 451.

(22) See ref 9, p 33 and references therein.

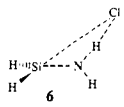
(23) Truong, T. N.; Gordon, M. S. *J. Am. Chem. Soc.* **1986**, *108*, 1775.

(24) Foster, J. M.; Boys, S. F. *Rev. Mod. Phys.* **1960**, *32*, 300.

(25) Nugent, W. A.; Mayer, J. M. *Metal-Ligand Multiple Bonds*; Wiley: New York, 1988.

(26) Rothwell, I. P. In *Activation and Functionalization of Alkanes*; Hill, C. L., Ed.; Wiley: New York, 1989; p 151.

(27) Numerous references to the original literature can be found in: Saillard, J.-Y.; Hoffmann, R. *J. Am. Chem. Soc.* **1984**, *106*, 2006.

Table III. Transition-State Geometries^a


H	M	MN	NH _t	H _t X	XM	MH _t	MNH _t	NH _t X	H _t XM	XMN	MNH _t
H	Ti	1.71	1.48	0.97	1.86	1.80	68	140	71	81	176
	Zr	1.86	1.52	0.97	2.06	1.97	71	144	71	74	178
	Hf	1.84	1.56	0.95	2.05	1.97	70	143	72	76	179
CH ₃	Si	1.63	1.53	0.92	1.75	1.74	67	134	74	84	133
	Ti	1.71	1.42	1.43	2.23	1.77	68	152	52	88	176
	Zr	1.86	1.44	1.43	2.44	1.94	71	157	53	80	179
NH ₂	Hf	1.85	1.46	1.41	2.42	1.93	70	156	53	81	179
	Si	1.63	1.45	1.32	2.13	1.75	69	148	55	89	135
	Ti	1.74	1.38	1.33	2.09	1.92	76	138	64	82	162
Cl	Zr	1.89	1.36	1.32	2.26	2.10	78	141	78	75	162
	Hf	1.87	1.40	1.30	2.22	2.08	77	140	66	76	163
	Si	1.65	1.43	1.22	1.87	1.75	78	124	75	83	133
SiH ₃	Ti	1.69	1.72	1.39	2.60	2.16	78	142	56	84	165
	Zr	1.84	1.80	1.37	2.83	2.38	82	144	57	78	167
	Hf	1.82	1.88	1.36	2.79	2.40	81	140	59	80	167
SiH ₃	Si ^b	1.60	1.30	1.53	3.86	2.52	120	176	23	40	123
	Ti	1.72	1.49	1.81	2.80	1.80	68	163	39	89	172
	Zr	1.86	1.53	1.80	3.02	1.98	72	168	39	82	176
SiH ₃	Hf	1.84	1.56	1.78	3.01	1.97	70	168	39	83	179
	Si	1.62	1.50	1.78	2.78	1.76	68	162	38	91	132

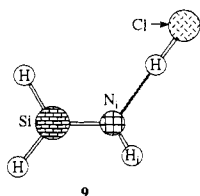
^a Calculated bond lengths (Å) and bond angles (deg) for the X-H elimination transition states. ^b The geometry of the TS for the elimination of HCl from (H)₂Si(Cl)(NH₂) is quite distinct from the others, looking quite like the H-bonded adduct 6.

Table IV. Calculated Energetics for X-H Elimination from TM Amidos^a

X	M	ΔH^*_{elim}	ΔH^*_{act}	ΔH_{rxn}
H	Ti	15.6	15.0	0.6
	Zr	26.1	11.9	14.2
	Hf	30.1	6.2	23.9
CH ₃	Si	84.9	44.0	40.9
	Ti	23.4	14.5	8.9
	Zr	34.1	14.1	20.0
NH ₂	Hf	38.0	7.3	30.7
	Si	83.3	39.4	43.9
	Ti	35.1	-6.2 (32.9) ^b	41.3 (2.2)
SiH ₃	Zr	41.1	-11.7 (25.8)	52.8 (15.3)
	Hf	44.3	-19.9 (21.5)	63.7 (22.3)
	Si	48.9	-11.5 (2.9)	60.4 (46.0)
Cl	Ti	17.5	15.5	2.0
	Zr	26.8	13.2	13.6
	Hf	30.4	7.5	22.9
Cl	Si	85.1	47.2	37.9
	Ti	49.5	-11.0 (2.5)	60.5 (47.0)
	Zr	58.9	-13.8 (-0.5)	72.7 (59.4)
Cl	Hf	64.7	-17.3 (1.9)	82.0 (66.6)
	Si	66.2	-5.7 (2.4)	72.0 (63.9)

^a Values are in kcal mol⁻¹ and were calculated at the MP2 level using RHF optimized geometries and RHF calculated zero-point energies. ΔH^*_{elim} is the enthalpic barrier for eq 1. ΔH^*_{act} is the enthalpic barrier for the microscopic reverse of eq 1, HX activation. ΔH_{rxn} is the enthalpy of reaction for eq 1. ^b Values in parentheses for X = NH₂ and Cl are those enthalpic data that take into account adduct formation between the imido and HX products; see eq 2. Values not in parentheses are versus separated reactants and products, eq 1.

kcal mol⁻¹ for the TMs and 14 kcal mol⁻¹ for Si. In HCl elimination, the adduct, 8, is ≈ 14 kcal mol⁻¹ more stable for M = Ti, Zr, and Hf. The Cl-H...N(H)=SiH₂ adduct, 9, is bound



by 8 kcal mol⁻¹. The geometries of the adducts are close to the individually optimized products, Table V, excepting the move

Table V. Geometries of NH₃ and HCl Adducts^a

	(H) ₂ M(NH)(HCl)					
	M=N	N...H	H-Cl	M...Cl	M=N-H	N...H-Cl
Ti	1.66	3.10	1.28	2.71	169	93
Zr	1.81	3.12	1.28	2.90	172	98
Hf	1.80	2.98	1.29	2.85	172	101
Si	1.59	1.92	1.31	4.35	121	179

	(H) ₂ M(NH)(NH ₃)			
	M←N	M=N	M=N-H	N←M=N
Ti	2.22	1.67	173	106
Zr	2.41	1.82	175	103
Hf	2.36	1.81	176	102
Si	2.05	1.60	123	107

^a Geometries of these Lewis acid and base adducts were calculated at the RHF level using the methods outlined in the text. See 6-8 for the general shape of these adducts. Bond distances in Å, angles in deg.

away from trigonal-planar coordination about the metal, as expected when the coordination number increases from 3 to 4.

Recent data for RH elimination from (NHSi')₃ZrR suggest that adduct formation between products is also a possibility even for very weak bases like alkanes.²⁹ Methane adducts of (H)₂M=NH (M = Ti, Zr, Hf) were calculated^{14b} to be bound by ≈ 9 kcal mol⁻¹, while a small binding enthalpy (1.3 kcal mol⁻¹) is found between H₂ and (NH₂)₂Zr=NH.⁷ Further elucidation of the structure and bonding of these weakly bound complexes is of interest, but was ignored in the present study except in the cases noted above where the eliminated molecule is a strong Lewis acid (HCl) or Lewis base (NH₃).

The calculated methane elimination barriers in (H)₂-M(NH₂)(CH₃) are 23.4 (M = Ti), 34.1 (M = Zr), and 38.0 (M = Hf) kcal mol⁻¹, in modest agreement with experiment: (OSi')₂(NHSi')Ti-CH₃ (≈ 21 kcal mol⁻¹),²⁸ (NHSi')₃ZrCH₃ (25.9(4) kcal mol⁻¹),²⁸ and (NHSi')₃Hf-CH₃ (30.0 kcal mol⁻¹), Si' = Si(*t*-Bu)₃.²⁸ More extensive studies of methane elimination^{14b} have shown that increases in the accuracy of the model (adding polarization functions to the H basis set, replacing hydrido with

(29) Sigma (or agostic) complexes, particularly of H₂ and silanes, are more well known for low-valent transition metal species, with examples being stable enough for structural characterization: Crabtree, R. H.; Hamilton, D. G. *Adv. Organomet. Chem.* 1988, 28, 299.

amido ancillary ligands, and correcting to the temperature at which the experimental determinations were made, $\approx 100^\circ\text{C}$) lowers the calculated $\Delta H_{\text{elim}}^{\ddagger}(\text{CH}_4)$ by roughly 4 kcal mol $^{-1}$, in improved agreement with experiment. More importantly, the experimental and computational data show the same trends in methane elimination barriers: $\text{Hf} > \text{Zr} > \text{Ti}$.²⁸

Some interesting points do emerge from the calculated ΔH_{rxn} . One can define $\Delta\Delta H_{\text{rxn}}(\text{M}-\text{M}')$ as the difference in ΔH_{rxn} for two metals (M and M') and a given leaving group, X. From the data in Table IV, these quantities are those given in eq 3–5.

$$\Delta\Delta H_{\text{rxn}}(\text{Zr}-\text{Ti}) = 10 \pm 1 \text{ kcal mol}^{-1} \quad (3)$$

$$\Delta\Delta H_{\text{rxn}}(\text{Hf}-\text{Ti}) = 12 \pm 1 \text{ kcal mol}^{-1} \quad (4)$$

$$\Delta\Delta H_{\text{rxn}}(\text{Hf}-\text{Zr}) = 22 \pm 1 \text{ kcal mol}^{-1} \quad (5)$$

The near constancy in $\Delta\Delta H_{\text{rxn}}$ for each of the five different leaving groups is striking. The reaction enthalpy can be estimated from the bond energies:

$$\Delta H_{\text{rxn}} \approx \text{BE}_{\text{M-X}} + \text{BE}_{\text{M-N}} + \text{BE}_{\text{N-H}} - \text{BE}_{\text{M=N}} - \text{BE}_{\text{H-X}} \quad (6)$$

One can define the difference between the MN amido and imido bond energies as the metal–nitrogen π -bond energy (Π_{MN}):

$$\Delta H_{\text{rxn}} \approx \text{BE}_{\text{M-X}} + \text{BE}_{\text{N-H}} - \Pi_{\text{MN}} - \text{BE}_{\text{H-X}} \quad (7)$$

For different metals and the same X, $\Delta\Delta H_{\text{rxn}}$ is as given in:

$$\Delta\Delta H_{\text{rxn}} \approx \Delta\text{BE}_{\text{M-X}} - \Delta\Pi_{\text{MN}} \quad (8)$$

The limited number of X groups and the uncertainty caused by the lack of comparable computational and experimental data does not allow us to assess the reasons why eq 8 should yield a near-constant value for a given pair of metals. Clearly, there is a need for further studies aimed at calculating reliable thermochemical data for molecular TM-MG materials, perhaps using a scheme similar to the G1 and G2 theories of Pople et al.³⁰ which routinely predicts main-group thermochemical data to within ± 2 kcal mol $^{-1}$. Currently, efforts are underway in our labs to predict the TM-MG thermochemistry at a comparable level of accuracy using a combination of all-electron and ECP wave functions.

3. Intrinsic Reaction Coordinate for HX Elimination. The intrinsic reaction coordinate (IRC)^{18,19} for the elimination of various HX from the transition metal amidos was studied in order to obtain some insight into the dynamics of the process. The specific case discussed here is H_2 elimination from $(\text{H}_3)\text{Hf}-\text{NH}_2$, but the other IRCs studied have revealed themselves to be fundamentally the same. A plot of the changes in pertinent bond lengths and bond angles along the IRC is shown in Figure 1. Internal coordinates which increase or decrease monotonically from reactant to product are not plotted in Figure 1. The mass-weighted distance along the reaction coordinate is denoted S_{total} with the TS located at $S_{\text{total}} = 0 \text{ bohr}\cdot\text{amu}^{1/2}$. As expected, the bond lengths showing the most dramatic changes are the H_a-H_i bond (H_a is the hydrogen originally bonded to Hf) of the H_2 being eliminated and the N_i-H_i bond (N_i is the imido nitrogen, 5) being cleaved. There are two points in Figure 1a where the slopes of the lines change significantly. The first of these occurs at roughly $S_{\text{total}} = -1.2 \text{ bohr}\cdot\text{amu}^{1/2}$. After $S_{\text{total}} = -1.2 \text{ bohr}\cdot\text{amu}^{1/2}$, the N_i-H_i bond, which up to this point is stretched little from the amido reactant, undergoes rapid elongation. As noted elsewhere⁷ the abrupt increase in the N_i-H_i bond length is roughly coincident with a leveling off of the $\text{M}-\text{N}_i-\text{H}_i$ angle (at $\approx 180^\circ$) while the $\text{M}-\text{N}_i-\text{H}_i$ angle is $\approx 75^\circ$, Figure 1b. In other words, up until $S_{\text{total}} \approx -1.2 \text{ bohr}\cdot\text{amu}^{1/2}$, the amido ligand is essentially just pivoting in place, **10a**, and thus resembles the isoelectronic agostic³¹ Ta-alkylidene,^{31a} **10b**, at $S_{\text{total}} \approx -1$

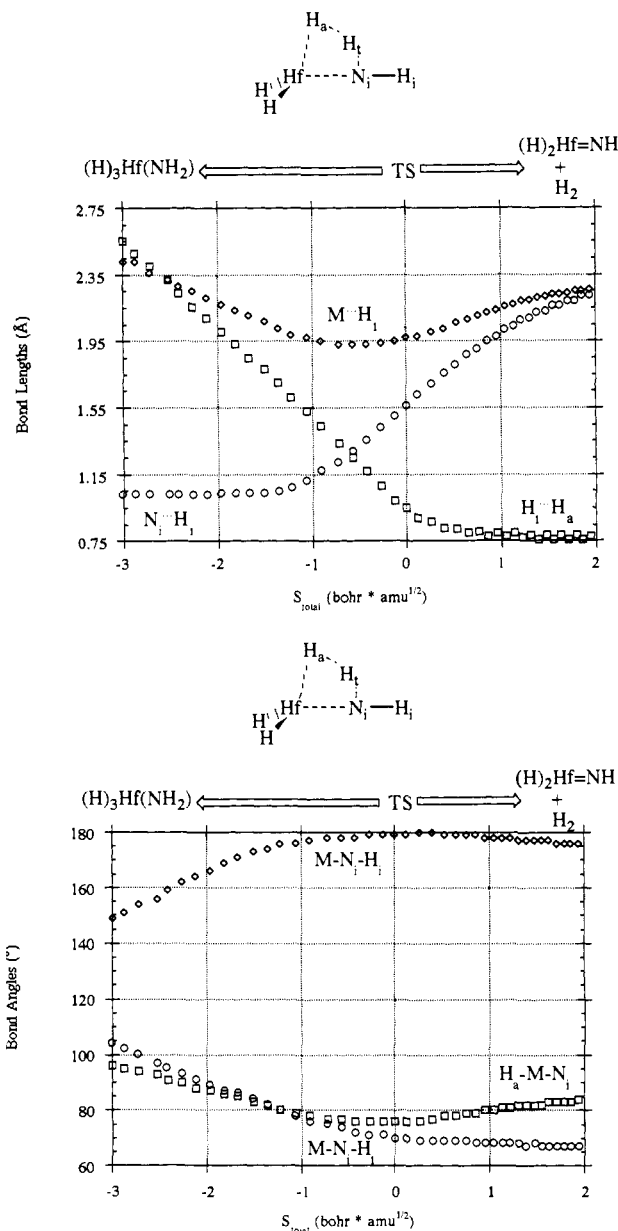
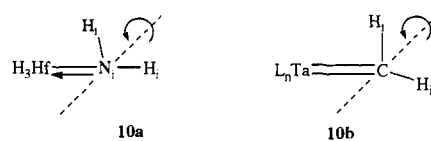


Figure 1. Plot of the changes in pertinent (a) bond lengths and (b) bond angles along the calculated IRC for the elimination of H_2 from $\text{H}_3\text{Hf}-\text{NH}_2$. The reactant (amido complex) is on the left; products (H_2 and imido) are on the right, and the TS is set to $S_{\text{total}} = 0 \text{ bohr}\cdot\text{amu}^{1/2}$.



bohr·amu^{1/2}. Recently, crystal structures of d^0 Zr-amido complexes with bulky N substituents ($\text{Zr}(\text{NHSi}^t)_3(\text{CH}_3)$ and $\text{Cp}^*\text{Zr}(\text{N}(\text{H})-t\text{-Bu})_3$) have been reported,^{31d} which show large ($\approx 160^\circ$) Zr-N-C angles, shorter than normal Zr-amido bonds ($\approx 2.00 \text{ \AA}$), and although H atoms were not located, one can presume small Zr-N-H angles. Thus, they are structurally analogous to the Ta-neopentylidenes of Schrock et al.^{31a} After $S_{\text{total}} \approx -1 \text{ bohr}\cdot\text{amu}^{1/2}$, N_i-H_i begins to lengthen considerably, while H_a-H_i shows an equally steep decrease as the H_2 molecule is formed. The second point at which there is a significant change in slope, Figure 1a, is at $S_{\text{total}} \approx 0.5 \text{ bohr}\cdot\text{amu}^{1/2}$; the H-H bond of H_2 is fully formed and no further compression takes place.

An additional point of interest in Figure 1 is the fact that, when the H_i-H_a and N_i-H_i lines cross (i.e., their internuclear

(30) (a) Pople, J. A.; Head-Gordon, M.; Fox, D. J.; Ragachavari, K.; Curtiss, L. A. *J. Chem. Phys.* 1989, 90, 5622. (b) Curtiss, L. A.; Ragachavari, K.; Trucks, G.; Pople, J. A. *J. Chem. Phys.* 1991, 94, 7221.

Table VI. Calculated Mulliken Bond Overlap Populations^a

M/X	BOP(MH _i)	BOP(MH _{term})	BOP(MH _i)/ BOP(MH _{term})
Ti/H	0.11	0.37	0.30
Ti/Me	0.09	0.37	0.24
Ti/SiH ₃	0.18	0.37	0.49
Ti/NH ₂	0.04	0.36	0.11
Ti/Cl	0.00	0.37	0.00
Zr/H	0.08	0.34	0.24
Zr/Me	0.07	0.34	0.21
Zr/SiH ₃	0.15	0.34	0.44
Zr/NH ₂	0.03	0.34	0.08
Zr/Cl	0.01	0.34	0.03
Hf/H	0.12	0.38	0.32
Hf/Me	0.11	0.38	0.29
Hf/SiH ₃	0.18	0.38	0.47
Hf/NH ₂	0.05	0.38	0.13
Hf/Cl	0.03	0.37	0.08

^a Being off-diagonal elements of the bond overlap population matrix, these values must be multiplied by two to get the total BOP for a specific pair. The ratio of BOP values will, of course, not change from the values quoted in column three.

separations are equal), the M–H_i distance is at its minimum. The coincidence of the MH_i minimum with the H_iX and N_iH_i crossing points, noted elsewhere,^{7,14b} seems to be a general feature of HX elimination reaction coordinates, and is discussed below.

Discussion

Several interesting points have emerged from the analysis of HX elimination, which may be of interest with regard to high-valent TM chemistry and the design of CVD precursors.

The most interesting structural features of the HX elimination TSs are the large angles about H_i, **5a**, and the short metal–transannular hydrogen (H_i) distances it engenders. Short MH_i distances have been observed previously in computational studies of HX activation by high-valent TM complexes.^{6,7,14b,32} By comparison with normal metal–terminal hydride (MH_{term}) bond lengths, Table III, it is evident that highly electronegative X groups result in considerably longer MH_i distances (12% and 28% greater for X = NH₂ and Cl, respectively, versus MH_{term}) than the other leaving groups (only ≈5% greater for X = H, SiH₃, CH₃ versus MH_{term}).³³ With the assumption that a shorter MH_i distance (for the same metal) indicates a stronger interaction, one can infer that the MH_i interaction is weaker in the transition metal TSs when X is a more electronegative group.

Evidence for a stabilizing MH_i interaction in the TS is found in the Mulliken bond overlap population (BOP),¹⁷ an indicator of the strength of interaction between two nuclei. For each transition metal TS we have calculated the BOP(MH_i) and scaled it relative to BOP(MH_{term}). These data are collected in Table VI. Note that the sign of the BOP is positive in all cases, indicating a stabilizing interaction. While BOP(MH_{term}) is insensitive to M and X modification, as expected, the BOP(MH_i) values vary widely, Table VI. This becomes clear when reduced bond orders (BOP(MH_i) + BOP(MH_{term})) are studied in Table VI; for the electropositive silyl leaving group, BOP(MH_i) is nearly one-half of BOP(MH_{term}), but less than one-tenth for electronegative chloro and amido leaving groups. Thus, the Mulliken BOPs indicate that the electronegative X groups engender a weaker stabilizing

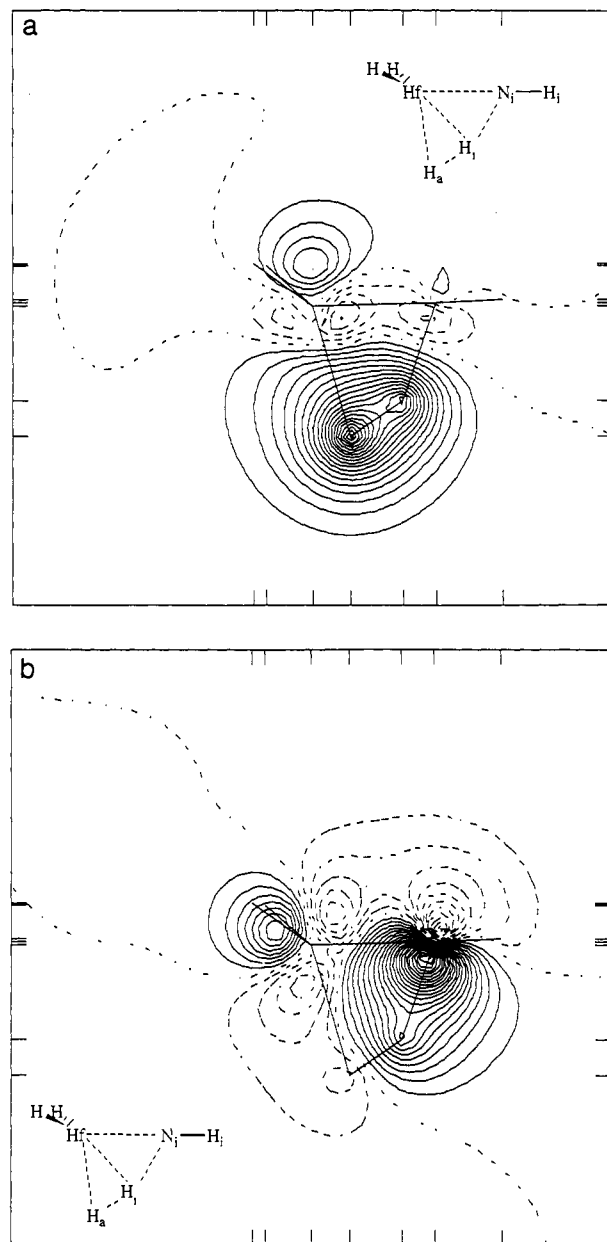


Figure 2. Boys localized MO from the TS for the elimination of H₂ from H₃Hf–NH₂. The MO in (a) is delocalized over Hf, H₁, and H_a. The MO in (b) is delocalized over Hf, Ni, and H₁. See text for percentages. The lowest contour is 0.02 bohr^{-3/2}; the increment between successive contours is 0.02 bohr^{-3/2}.

interaction between the metal and H_i in the TS, in concurrence with the longer MH_i distances seen for these transition states.

We have plotted in Figure 2 typical examples of the localized MOs for the atoms comprising the four-center TS; H₂ elimination from H₃Hf–NH₂ is used in Figure 2. Each of the two MOs shown in Figure 2 is spread over three atoms, in contrast to the two-center/two-electron localized MOs usually obtained for stable ground-state species. A Mulliken population analysis indicates that the localized MO in Figure 2a is 24% Hf, 23% H₁, and 53% H_a; the localized MO in Figure 2b is 18% Hf, 70% Ni, and 12% H₁. The delocalization of these MOs raises the possibility that the MH_i interaction may be significantly “through-bond” (i.e., mediated by the AOs of the intervening atoms N_i and X) as well as “through-space”. Although there is a degree of arbitrariness in examining a particular set of (localized) orbitals, this picture provides a convenient explanation of the sensitivity of the MH_i distance (and hence the strength of their interaction) to the X group. In Figure 3, the total electron density is plotted in the

(31) (a) Schrock, R. R. *Acc. Chem. Res.* **1979**, *12*, 98. (b) Green, M. L. H.; Brookhart, M.; Wong, L. K. *Prog. Inorg. Chem.* **1988**, *36*, 1. (c) Hoffmann et al. present an analysis of the electronic factors controlling the distortion of the alkylidene group in Ta–alkylidenes from normal to agostic coordination: Hoffmann, R.; Jemmis, E.; Goddard, R. J. *J. Am. Chem. Soc.* **1980**, *102*, 7667. (d) Bai, Y.; Roesky, H.; Noltemeyer, M.; Witt, M. *Chem. Ber.* **1992**, *125*, 825. Cummins, C. C.; van Duynne, G. D.; Schaller, C. P.; Wolczanski, P. T. *Organometallics* **1991**, *10*, 164.

(32) (a) Goddard, W. A.; Steigerwald, M. L. *J. Am. Chem. Soc.* **1984**, *106*, 308. (b) Rappé, A. K. *Organometallics* **1990**, *9*, 466. (c) Hoffmann, R.; Saillard, J.-Y.; Rabañá, H. *J. Am. Chem. Soc.* **1986**, *108*, 4327.

(33) Note that other than the anomalous X = Cl transition state, Table III, the Si analogues are quite insensitive to X modification.

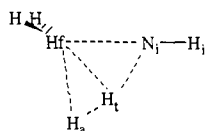
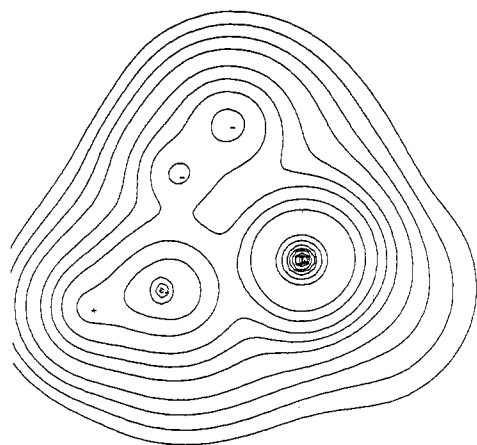


Figure 3. Plot of total electron density in the plane of the four atoms which make up the four-centered TS (i.e., Hf, Ni, Hi, and Ha). The lowest contour is $0.05 \text{ bohr}^{-3/2}$; the increment between successive contours is $0.05 \text{ bohr}^{-3/2}$.

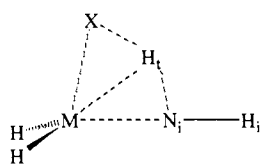
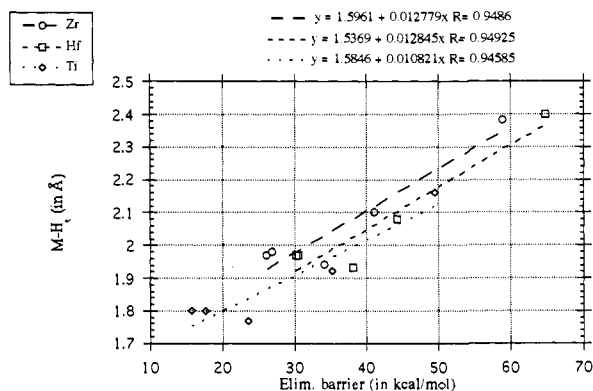


Figure 4. Plot of the calculated elimination barrier versus MH_i distance in the optimized transition state. The least-squares line for each of the transition metals is drawn and the equation for each denoted.

plane of the four atoms which comprise the [2 + 2] TS (Hf, Ni, Hi, and Ha), showing that the electron density is accumulated more along the edges of the four-centered TS than in the center.

From the data in Table IV it can be seen that more electronegative X groups have higher elimination barriers. A plot of the calculated $\Delta H^\ddagger_{\text{elim}}$ versus MH_i distance (as a function of X for a given TM) in the 1,2-elimination TSs, Figure 4, does yield a reasonably straight line ($R \approx 0.95$). Clearly, both thermodynamic and kinetic factors will be at work, but stronger MH_i interaction (as deduced from a shorter MH_i distance) seems to correlate with lower activation barriers to HX elimination. This further supports the notion that the metal-transannular hydrogen interaction is playing an important role in modifying the structure and energetics of the TS in HX elimination, and that this interaction is mediated by the leaving group.

An analysis of the intrinsic reaction coordinate (IRC),

illustrated in Figure 1, indicates that HX elimination occurs in two stages.^{7,14b} First, there is a compression of the $X-M-N_i$ angle while the NH_2 ligand pivots in place, to form one large (i.e., $M-N_i-H_i \gg 120^\circ$) and one small (i.e., $M-N_i-H_i \ll 120^\circ$) angle, as shown in 10a and Figure 1a. Once these motions have taken place, the $N-H_i$ bond lengthens, H_i is transferred to X, and HX is eliminated, Figure 1a. The fact that $N-H_i$ does not lengthen until the amido has pivoted strongly suggests that the pivoting motion is necessary in order to prepare the $N-H_i$ bond for cleavage. In the region of the IRC near $S_{\text{total}} \approx -1.2 \text{ bohr-amu}^{1/2}$, the Mulliken BOP is significantly greater for the spectator N_i-H_a bond (BOP ≈ 0.70) than the N_i-H_i bond (BOP ≈ 0.45) despite the similarity in bond lengths ($N_i-H_i > H_i-H_i$ by $0.05\text{--}0.07 \text{ \AA}$). The difference in calculated BOPs suggests the N_i-H_i bond is considerably weaker than N_i-H_a and the initial N_i-H_i in the amido reactant.

The structural similarity between the TM-amido moiety at the end of the pivoting motion, and reported neutron diffraction structures^{31a} for isoelectronic Ta-alkylidenes, leads us to suspect that some interaction occurs between the N_i-H_i bond and the electrophilic metal. Calculation of atomic charges from the Mulliken population analysis supports this assertion, showing electrons flowing from N_i-H_i (N_i from -1.05 to -0.91 and H_i $+0.31$ to $+0.35$) to the metal, which becomes less positively charged ($+0.96$ to $+0.72$ in our H_3Hf-NH_2 example). Localization of the MOs at this point shows the N_i-H_i bond to be delocalized to some extent onto the metal (e.g., 9% Hf, 58% Ni, and 33% H_i in H_3Hf-NH_2). The extent of metal delocalization is less than in the TS (vide supra) but greater than in the amido minima. Agostic $X-H \cdots M$ interactions have been envisaged as precursors to the activation of $X-H$ and thus have attracted considerable experimental interest, particularly when $X = C$.^{31,34} The intrinsic reaction coordinate supports the experimental contention that agostic bonding does precede activation and suggest that even if it does not exist as an equilibrium structure in a reactant (as the smoothness of the present IRCs indicate) that it may still take place along the reaction coordinate. Moreover, the calculations further suggest that this agostic interaction does indeed facilitate the subsequent scission of the $N-H$ bond.

The second interesting result from the IRC analysis is that the MH_i distance decreases as the reactants move toward the TS, reaches a minimum value, and then increases as the reaction proceeds further, Figure 1. This gives the curve, which describes the changes in the MH_i distance along the IRC, a parabolic shape, with the minimum coincident with the crossing point at which the H_a-H_i bond being formed and the N_i-H_i bond being broken are equal in length. The coincidence between these points seems to be a general phenomenon in all IRCs for HX activation/elimination from TM amido complexes that we have studied.^{7,14b} One can interpret this as additional evidence that the MH_i interaction is important in stabilizing the TS and thus moderating the elimination barrier. Note also that the curve which describes the changes in the calculated BOP(MH_i) shows the opposite trend to the MH_i curve in Figure 1a; i.e., it increases from reactants toward TS and then decreases as the IRC approaches products. The transition metal thus appears to develop significant bonding interaction with H_i making the transition state more energetically accessible than in a case where this interaction is unfavorable. Thus, one can describe the elimination process as a "metal-mediated H-transfer."³⁵ It seems reasonable to infer that low-energy, vacant d orbitals on the TM are the source of the interaction with H_i in the TS and along the IRC for elimination. Consistent with this hypothesis are the much higher $\Delta H^\ddagger_{\text{elim}}$ for Si which has no low-energy d orbitals. Additional support for this conclusion comes from the d-orbital Mulliken populations

(34) Crabtree, R. H. *Chem. Rev.* 1985, 85, 245.

(35) We thank Professor Dave Wigley (Arizona) for providing this illustrative description of the reaction coordinate.

for the Si species, which is considerably smaller than their TM counterparts ($\approx 0.5 e^-$ versus $\approx 2.0 e^-$).

If one wishes to deposit a film or structure with the composition M_xE_y , then the choice of the best precursor will entail optimal design of the leaving group (X) and/or the ancillary ligands (L_n). The late TS means that the H-X bond is nearly fully formed and interaction between these two centers is significant, allowing the leaving group to intimately influence the relative nucleophilicity/electrophilicity of H_i . The localized MOs suggest that this interaction is mediated by a three-center/two-electron ("through-bond") interaction among the metal, X and H_i . The calculations suggest that the more readily the TM can stabilize H_i (in the TS and along the IRC), the lower the barrier to elimination of HX will be. Clearly, thermodynamic effects are expected to contribute to this picture as well, but the present calculations suggest that there is a significant amount of kinetic control on the elimination process. The calculations lead to the conclusion that TM-MG materials precursors which are designed to enhance the MH_i interaction will lead to lower activation barriers to XH elimination and presumably lower processing temperatures or higher rates at a given temperature.

Acknowledgment. This work was supported in part through a grant from the Air Force Office of Scientific Research (to M.S.G., 90-0052) and a Faculty Research Grant (to T.R.C.) from Memphis State. Calculations were carried out on a DECstation 5000/200 at Memphis State (a generous loan from the Digital Equipment Corp.), an IBM RS-6000/530 (purchased in part by a grant from the National Science Foundation to M.S.G. while at North Dakota State University), and the iPSC/860 at Oak Ridge National Laboratories (made available through participation of the Computational Chemistry Group at MSU in the Joint Institute for Computational Science located at University of Tennessee-Knoxville). Several of the larger calculations were run on the Cray Y-MP4/464 at the National Center for Supercomputing Applications, administered by the NSF, through Grant CHE920026N to T.R.C. The authors thank Professor S. Ted Oyama (Clarkson) for providing reprints and preprints of his papers, Professor Peter T. Wolczanski (Cornell) for supplying experimental data prior to publication, and Dr. Steven K. Showalter (Sandia) for informative discussions about experimental aspects of CVD and materials processing.